Advancements in Emerging MXene-Integrated Nanocomposite Coatings: Unraveling Defect-Free Microstructure for Superior Tribological, Mechanical, and Anti-Aging Features

Xingyu Wang [a], Sampada Koirala [b], Luyang Xu [a], Qiaobin Li [d], Danling Wang [b], Xiaoning Qi [c], Ying Huang [a], Zhongyu Yang [d], and Zhibin Lin [a]*

[a] *Department of Civil, Construction, and Environmental Engineering, North Dakota State University, Fargo, ND 58108, USA*

[b] *Department of Electrical and Computer Engineering, North Dakota State University, Fargo 58108, ND, USA*

[c] *Department of Coatings and Polymeric Materials, North Dakota State University, Fargo, ND 58018, USA*

[d] *Department of Chemistry and Biochemistry, North Dakota State University, Fargo, ND 58108, USA*

** Corresponding author: North Dakota State University, 1340 Administration Ave., Fargo, ND 58108, USA, Email: zhibin.lin@ndsu.edu; Phone:701-231-7204.*

Abstract

This study explored the enhancement potential of MXene, a novel two-dimensional material, in epoxy-based nanocomposites; which comprehensively examined the influence of MXene on epoxy's viscosity, void formation, aging resistance, mechanical properties, and anti-wear properties. MXene nanofillers, labeled as 25C and 80C, fabricated via different acid-etching methods, were incorporated into epoxy resin at varying weight percentages (0.1-2.0 wt.%). Observations revealed that for both varieties of MXene, inclusion of 1.0 wt.% MXene led to the mitigation of void content, whereas the incorporation of 2.0 wt.% MXene yielded maximal enhancements in both tensile strength and abrasion resistance. Additionally, the integration of 1.0 and 2.0 wt.% MXene displayed superior aging resistance, with around 80% reduction in free radical formation compared to the unmodified epoxy, while maintaining its excellent mechanical properties after QUV exposure. Therefore, both MXene types significantly enhanced the performance of epoxy composites, with the 80C-MXene displaying marginally superior enhancement due to its smaller particle size and higher purity, as identified by SEM and TEM images.

Keywords: MXene, Polymer-matrix composites (PMCs), Mechanical properties, Microstructures, Anti-aging

1. Introduction

MXenes are a class of two-dimensional (2D) transition metal carbides, nitrides, and carbonitrides that are promising materials for a wide range of applications, from energy storage to advanced composite materials [1–5]. The unique combination of properties in MXene nanoflakes, including high conductivity, hydrophilicity, and functional ability, has drawn the attention of scientists from different disciplines [6]. Recently, in materials science, MXenes are being explored as potential nanofillers in polymer composites because of their excellent mechanical strength and compatibility with various polymers [6].

Polymeric materials are versatile and easy to process, making them essential in many industries, including automotive, aerospace, and electronics. However, the limitations of pure polymer composites in mechanical and anti-wear properties restrict their potential applications. Additionally, the performance of polymeric materials often degrades over time due to aging effects, leading to a loss of integrity and efficiency, which is a significant challenge to be addressed. Therefore, although polymers are widely used due to their good performance, processability, and cost-effectiveness [7–9], traditional polymer materials often fail to meet the demands of certain applications, particularly those requiring high mechanical strength, wear resistance, and long-term durability [10–13]. Those challenges have led to research efforts aimed at enhancing the mechanical durability and aging resistance of polymeric materials.

MXenes have emerged as a potential solution to these challenges above; their exceptional mechanical properties and unique geometric shapes make them suitable nanofillers for enhancing the performance of polymers [1,14,15]. Moreover, MXenes' compatibility with various polymers and their hydrophilic nature allow for improved dispersion within the polymer matrix, leading to a more effective reinforcement effect [16]. The incorporation of MXenes into polymer matrices is expected to confer the resulting composites with enhanced mechanical, anti-wear, and other protection properties [17–19], and this enhanced properties would significantly broaden the applications of polymer materials [6].

One challenge of using MXenes is their susceptibility to oxidation in the air, led to the formation of TiO_2; another challenge is that MXenes are prone to restacking after dispersion. Both of these challenges can be overcome by using MXenes as nanofillers and directly dispersing them into polymeric resin: the oxidization of MXenes will be inhibited as they are covered by polymeric matrix, and the high viscosity of polymeric resin will mitigate dispersed MXene flakes from restacking. Therefore, the application of MXene into polymeric coating shows great potential and recent years have seen an increased interest in MXene-based composites, as evidenced by the exponential growth in the number of published research papers [20–25]. For example, Yan presented a study on using $Ti_3C_2T_x$ sheets to prepare composite coatings with good dispersity and interface interaction in waterborne epoxy coating. The MXene-epoxy coatings with 0.5 wt.% optimal addition exhibited the best corrosion and tribological performance due to well-dispersed amino-functionalized $Ti_3C_2T_x$ sheets and the formation of a tortuous network in the epoxy coating. The study shows that the addition of amino-functionalized $Ti_3C_2T_x$ sheets can significantly improve its properties, providing a potential solution for

corrosion and wear resistance [26]. Zeng et al. performed a study that synthesized $Ti_3C_2T_x$ MXene nanocomposites using a silane coupling agent, resulting in improved dielectric and mechanical properties. The nanocomposites showed a high dielectric constant and low dielectric loss, as well as increased tensile strength and elongation at break. Previous research has introduced a new approach to prepare polymer-based dielectric materials with practical applications [27]. Results from other studies also concluded that the application of MXene into polymeric coating can significantly improve the mechanical, anti-wear, and protection properties of polymeric materials, therefore a novel approach for interdisciplinary research in the development of advanced materials by incorporating MXene nanoparticles [28–34]. Chen et al. conducted studies on the impact of $Ti_3C_2T_x$ MXene on the mechanical and tribological properties of polymeric matrices, notably incorporating $Ti_3C_2T_x$ MXene with MoS_2 to create hybrids that enhanced bismaleimide composites [35]. The inclusion of these hybrids in bismaleimide (BMI) composites markedly improved mechanical strength, increasing impact and flexural strengths by 85% and 42% respectively, and reduced friction and wear, decreasing the frictional coefficient and wear rate by 69% and 88%. These results highlight the potential of using MXene/MoS_2 hybrids as high-performance lubrication additives in polymer matrices. In addition, MXene was effectively combined with graphene oxide, functionalized with Si-O-C hyperbranched polysiloxane (HBPSi-1, 2, 3), leading to enhanced interfacial adhesion with the epoxy matrix [14]. This graphene oxide/MXene (RGO/MXene) hybrid demonstrated significant improvements in both mechanical and frictional performance of the composites, indicating its promise as a solid lubricant additive for advanced material applications. These investigations have highlighted the promise of MXene-polymer composites and reported significant enhancements in composite properties upon the integration of MXene. The analysis of the Web of Science data indicates an exceptional increase in the prevalence of "MXene & polymer" and "MXene & high-performance" within scientific publications in recent years, which means an exponential expansion of this research field (as depicted in Fig. 1).

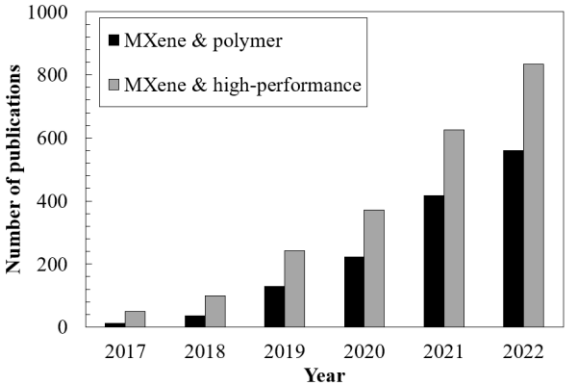

Figure 1. The scientific publications with the keywords of "MXene & polymer" and "MXene & high-performance", results were obtained from the Web of Science.

Nevertheless, despite these advances, our understanding of the effects of MXene addition on the aging behavior of polymer composites is still relatively limited. Given the critical importance of aging resistance for the durability and longevity of polymeric materials in practical applications, this crucial knowledge gap that must be addressed. By exploring how MXene as a nanofiller affects the aging behavior of polymer composites, researchers can improve their performance and increase their lifespan, making the new composites suitable for a wider range of applications.

Therefore, this study seeks to explore the reinforcing effects of MXene by offering a comprehensive analysis of the interactions between MXene and the polymer matrix, as well as their implications on composite performance. Specifically, in view of the mentioned prospects and challenges, this study investigated the effect of MXene reinforcement on the microstructure, mechanical, anti-wear, and anti-aging properties of epoxy-based nanocomposites. MXene nanoflakes, noted as 25C and 80C, were synthesized using various acid-etching techniques, and both of them were subsequently integrated into epoxy resin at different weight percentages ranging from 0.1 to 2.0 wt.%. The assessment of the role of MXene content on the void structure and the anti-aging properties were achieved by employing advanced characterization techniques, such as Micro-CT scanning and Electron Spin Resonance (ESR) spectroscopy. In addition to the ESR spectroscopy, the anti-aging ability of MXene-epoxy composites was also characterized by mechanical properties degradation after exposure to an accelerated environment test. Therefore, the insights derived from our research could guide the design and synthesis of high-performance, durable polymer composites, and facilitate the widespread adoption of MXene-polymer composites across various industries.

2. Materials and experimental design

2.1. Synthesis of $Ti_3C_2T_x$ MXene

MAX powder synthesis:

Titanium aluminum carbide (Ti_3AlC_2) MAX phase was prepared by ball milling an equimolar mixture of titanium carbide (TiC), titanium (Ti), and aluminum (Al) for two hours. The milled powder was subsequently compacted into a pellet and sintered at 1350°C for four hours under an argon atmosphere. The sintered pellets were milled into powder and sieved through a 160-mesh screen.

MXene nanoparticles synthesis:

Two distinct methods were employed for the synthesis of MXene nanoparticles, and the final product namely as 25C and 80C MXene. *1) 25C MXene:* The minimally intensive layer delamination (MILD) method was used at ambient temperature without heating. Fluoride-based salt etchants were utilized to produce in-situ HF by mixing 1.6 g of lithium fluoride (LiF) with 15 mL of hydrochloric acid (HCl) and 5 mL of deionized (DI) water. The mixture was stirred for 5 minutes, after which 1.0 g of Ti_3AlC_2 powder was incrementally added and the reaction allowed to proceed for 48 hours at room temperature (25°C). 2) 80C MXene: The hydrothermal approach was employed for 80C MXene synthesis. A solution of LiF, HCl, and MAX in the ratio necessary for in-situ HF formation was stirred at room temperature for one hour. The solution was then transferred to an autoclave and heated to 80°C for 48 hours in a tube furnace.

Final washing and drying step for 25C and 80C: Following the 48-hour etching process, the acidic mixtures were washed multiple times with DI water via centrifugation (6000 rpm, 5 minutes per cycle). This washing process continued until a pH of 4-5 was achieved, indicating successful washing. Initially, the Ti_3C_2 paste is cleansed using ethanol in a centrifuge tube through centrifugation for 5 minutes at 6000 rpm. Subsequently, the paste can be left to dry in a vacuum oven for 24 hours. Once dried, the sample is transferred to a mortar for grinding into a fine powder, which is then stored in a glass vial for future use.

2.2. Fabrication of nanocomposite and specimen preparation

The fabrication of nanocomposites in this study utilized EPON 828, a bisphenol resin, and EPIKURE Curing Agent 3175 as the cross-linking agent, both of them were manufactured by Hexion in the United States. The sample fabrication process, illustrated in Fig. 2, involved dispersing MXene nanoparticles in the epoxy resin through a combination of high-shear mixing and ultrasonic dispersion. Firstly, the MXene nanoparticles

were dispersed into epoxy resin using a high-shear disk mixer at a controlled speed of 4000 rpm for 30 minutes. Then, the mixture was sonicated using a Misonix S1805 ultrasonic system, following a 15-second "on/off" cycle at 100% amplitude for a total of 30 minutes. To avoid overheating during the dispersion process, the mixture was placed in a water bath. After the dispersion process, the curing agent was incorporated into the mixture, maintaining a 1:1 mole ratio between the resin and the curing agent, and the total mixture was mechanically mixed for 10 minutes at a speed of 600 rpm.

Nanocomposites were fabricated with varying weight contents of the MXene nanoparticles, specifically 0.1, 0.5, 1.0, and 2.0 wt.%. All sample groups were labeled according to the type and quantity of MXene nanoparticles used. For instance, 0.5%25C-E and 0.5%80C-E represent composites reinforced with 0.5% by weight of 25C and 80C MXene, respectively. Additionally, pure epoxy samples were prepared as a reference group.

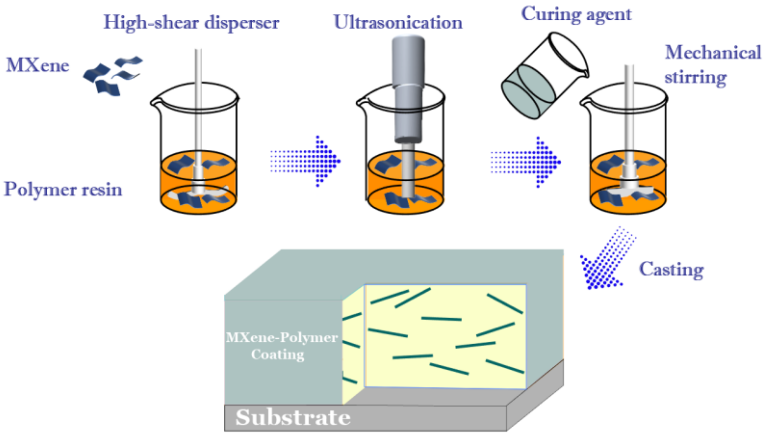

Figure 2. Schematic of the fabrication process of MXene-polymer nanocomposite.

2.3. Characterization techniques

Powder X-Ray Diffraction (XRD) patterns were captured by a Bruker AXS' D8 Discover multifunctional X-Ray Diffractometer, and the results were utilized to examine the structure of the MXenes. The micrographs that used in this study were produced with a field emission scanning electron microscope (FE-SEM), which a JSM-7600F Schottky was used. After tensile and abrasion testing, images of fractured and abraded surfaces were captured, providing insight into the microstructure of polymer matrix with and without nanoparticles, hence characterizing surface texture and fracture resistance. In addition, a high-resolution analytical TEM equipment, JEM-2100, was employed to analyze the morphology and structures of the MXene nanoparticles.

Once nanofillers were dispersed into the resin, viscosity test was conducted using a Brookfield DV-II viscometer in order to analyze the effect of nanofillers on the rheological behavior of the polymeric matrix.

2.4. Microstructure of nanocomposites: Micro-CT

Micro-CT, or micro-computed tomography, is a nondestructive imaging technology used to examine and analyze the internal structure of composite materials with a high degree of resolution. Micro-CT operates by employing X-ray radiation to generate a sequence of cross-sectional pictures of the sample, which are used to create a three-dimensional model of the sample. A Micro-CT scan was used to assess the defect/voids in the nanocomposite in order to examine the interactions between nanofiller and polymeric resin as well as the mechanisms of nanoparticle reinforcement. The investigation was conducted based on the void content and size distribution of the voids; the acquired data were then discussed together with the coating performance.

2.5. Accelerated weathering: QUV test

The OUV test was conducted to test the aging effect of nanocomposite under accelerated natural environment conditions. The QUV accelerated weathering test is a laboratory simulation method designed to assess the stability and durability of materials and coatings under conditions that mimic natural outdoor exposure. The samples were exposed to a rigorously controlled environment that reproduces the impact of sunlight, rainfall, and temperature fluctuations. The specimens were subjected to artificially accelerated weathering cycles that consist of a 4-hours UV-light irradiation with an irradiance of 0.71W m^{-2} and at an elevated temperature of 60 °C, followed by a 4-hours water condensation at 50 °C.

2.6. Mechanical properties: coupon tensile test

The tensile properties of the developed nanocomposite were determined using coupon tensile tests in accordance with ASTM D638. The dog-bone tensile test involves applying tension to a dog-bone-shaped sample until it fractures; and enables the evaluation of a material's mechanical properties under tensile stress. The coupons were clamped at both ends and loaded by Shimadzu's EZ-X tester at a rate of 1.0 mm/min, while the applied load and strain were recorded. Consequently, with the measured original cross-sectional area (A_0), the tensile strength ($f = \frac{P}{A_0}$) and ultimate strain of the specimens can be calculated using the load versus strain curve ($\varepsilon = \frac{L_0 - L}{L_0}$), where f is the applied load, and L_0 and L are the length before and after test.

2.7. Wear resistance: Taber abraser test

The abrasion resistance of the coatings was investigated using the Taber abrasive technique in accordance with ASTM D 4060, using 4*4" coated samples. The Taber abraser test is a technique to evaluate the ability of polymeric composites to abrasion forces. In this abrasion test, a coated substrate sample with a thickness of 310 ± 45 µm was subjected to a rotating abrasive wheel under a specific load. The coated surface rotates at 72 revolutions per minute under two CS-10 abrasive wheels. The abrasion test consisting of 1000 abrasive cycles, with a applied weight of 1000 grams on the wheels. The resistance of the coatings to abrasion is characterized by measuring the mass loss resulting from this process.

3. Result and discussion

3.1. Morphologies of fabricated MXene nanoparticles

As presented in Fig. 3, the findings from the XRD, Scanning Electron Microscopy (SEM), and Transmission Electron Microscopy (TEM) analyses provide substantial insight into the morphological characteristics of the 25C and 80C MXene samples and their impact on the overall properties of the formed composites.

The X-ray diffraction (XRD) patterns depicted in Fig. 3(a) provide a comparative analysis of MXenes synthesized via different methods. For the 80C MXene, the distinct (002) peak observed at 7.087° signifies a typical MXene structure [36]. Furthermore, the (004) peaks at 14.311° affirm the presence of MXene. At 80°C, the MXene XRD profile is dominated by a pronounced peak, with minimal evidence of residual Al and TiC phases. This suggests a thorough etching process where aluminum is effectively removed from the MXene layers. The presence of -OH as the surface terminating groups, indicated by the strong MXene peak, confirms a successful synthesis with a high degree of purity. This peak is a clear testament to the quality of the MXene, showcasing that the higher synthesis temperature optimizes the etching, allowing for the replacement of aluminum with hydroxyl groups on the MXene surface [37]. Conversely, the MXene synthesized at the lower temperature of 25°C exhibits a substantially weaker (002) peak, suggesting a less defined MXene phase. The presence of TiC impurities is confirmed by peaks at 35.985° and 44.96°, these findings indicate incomplete etching at this lower temperature, leading to lower quality MXene with significant TiC residue, as indicated by the broad and weak peaks between 40–50° [38].

In concordance with Scanning Electron Microscopy (SEM) analysis, the XRD results show that the sample synthesized at 80°C exhibits a more pronounced MXene characteristic peak, suggesting a higher quality of MXene. The corresponded SEM images of MXene distinctly showcase the formation of both 25C and 80C exfoliated MXene sheets, signifying the successful removal of the aluminum layer from the MAX phase. The images confirm the existence of a lamellar structure in both types of MXene flakes, which have extremely thin layer with uniform thickness. These uniform 2D nanostructured materials provide a high surface-to-volume ratio, which is a crucial property for improving chemical and physical properties [39]. However, observations from closer images reveal differences between the 25C and 80C MXene samples. As presented in Fig. 3(a), the 25C MXene sample exhibits a higher concentration of residual MAX phase particles than its 80C, suggesting the 80C samples have higher purity.

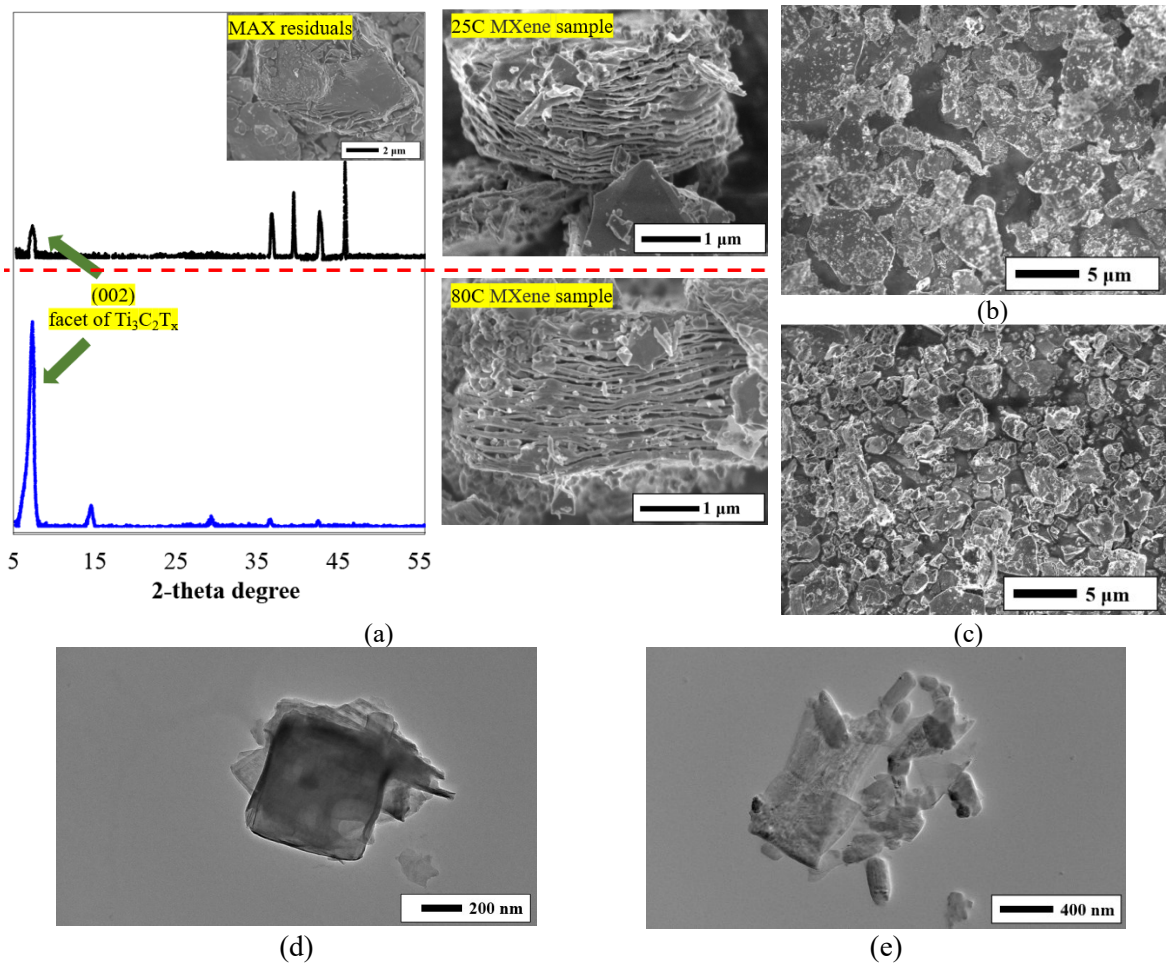

Figure 3. (a) XRD and corresponding SEM images of typical 25C and 80C MXene samples. Overview of (b) 25C MXene particles and (c) 80C particles. TEM images of 80C MXene nanosheets (d) before and (e) after ultrasonication.

Field Emission Scanning Electron Microscopy (FESEM) images in Fig. 3(b) and (c) pointed out the superior homogeneity and the smaller particle size of the 80C MXene samples. As observed in Fig. 3(b), the 25C MXene generally has a particle size larger than 5 μm while the 80C ones are smaller. Nanoparticles with smaller and well-distributed sizes can have improved dispersion, potentially providing a superior performance of composite that is reinforced by 80C MXene. Conversely, poor nanoparticle dispersion can lead to agglomeration, negatively impacting the material's performance [40,41], which may be the case for 25C MXene samples. On the other hand, TEM images in Fig. 3(d) and (e) depict a transformation in the 80C MXene sheets post-ultrasonication. The originally stacked square-shaped MXene sheets were effectively separated into individual, ultra-thin flakes after the ultrasonication process, offering increased surface areas and reducing the risks of agglomeration.

3.2. Viscosity of MXene-based nanocomposite

The objective of the viscosity test was to investigate the influence of the 25C and 80C MXene nanoparticles on the viscosity of epoxy resin under fluid state. As stated in the sample fabrication process, both of the MXene nanoparticles were added at four different concentrations, which were 0.1, 0.5, 1.0, and 2.0 wt.%. Apparently, it is essential to evaluate the impact of MXene nanoparticles' distinctive 2D morphology on the viscosity of the polymeric matrix. The 2D structure of MXene nanoparticles plays a vital role in the interactions between the epoxy and the nanoparticles, which potentially results in improved dispersion at lower concentrations or clumping at higher concentrations. Therefore, the incorporation of MXene nanoparticles might have either a positive or negative influence on the viscosity, and the interaction between them is discussed based on the results from the investigations below.

As presented in Fig. 4, the viscosity of the MXene-epoxy nanocomposites was measured. The obtained results were compared to the viscosity of the pure epoxy, which was used as a reference and had a value of around 22,000 cP. Apparently, it is evident that the addition of both types of MXene nanoparticles to the epoxy matrix has a significant impact on its viscosity. For both 25C and 80C MXene types, the viscosity of the mixtures was reduced when lower concentrations (0.1%, 0.5%, and 1.0%) of nanoparticles were incorporated. This reduction in viscosity may be attributed to the great dispersion of the 2D nanoparticles throughout the epoxy matrix. With the high degree exfoliation and dispersion of the nanoparticles within the matrix, allowing the particles to slide past each other more easily and causing the lubricant. The 2D MXene structures play the

role of solid lubricant as they are easy to be broken up by dynamic shear stresses [42]. As a result, the resistance against the flow is reduced, culminating in a lower viscosity in the mixtures. However, the viscosity of the MXene-epoxy mixtures increases substantially for both types of nanoparticles when 2.0% of nanoparticles were added. This increase in viscosity may be attributed to the agglomeration of the nanoparticles, which hinders the flow of the epoxy resin. The other reason is that the space between nanoparticles is reduced, which decreases the mobility of nanoparticles and increases the flow resistance of the mixture [43].

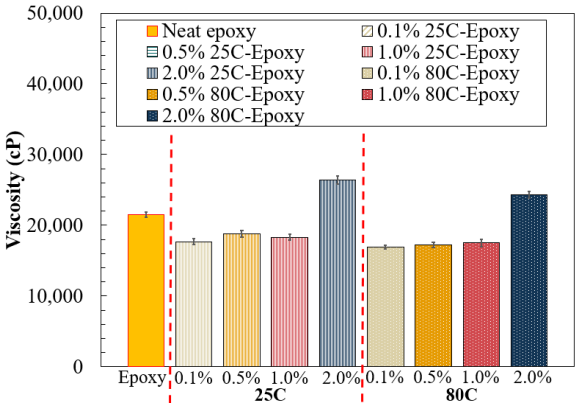

Figure 4. Viscosity of MXene-epoxy nanocomposite.

Nevertheless, when comparing the results for 25C and 80C MXene, it is obvious that the 80C MXene provides a stronger ability to reduce the viscosity of epoxy resin at low concentration levels (0.1 to 1.0 wt.%). Nanoparticles like 0.1% MXene can enhance fluid mobility in resin matrices through their lubricating effect. However, this effect has limits and does not linearly decrease viscosity with increased MXene content; as observed, additions of 0.5% and 1.0% MXene did not significantly improve viscosity. Conversely, at higher concentrations, such as 2.0%, the lubricant effect is negated due to the reduced space between particles, which hinders mobility and increases the dispersion's resistance to flow. Consequently, viscosity increases, particularly at concentrations above 1%. At these elevated nanoparticle levels, the MXene negatively impacts the viscosity of epoxy resins. Excessive particle loading in polymeric matrices leads to notable agglomeration, driven by nanoparticle-nanoparticle interactions, which further escalates viscosity and impairs fluid mobility [44]. This observation implies that the interaction occurring between the 80C MXene nanoparticles and the epoxy might be more favorable compared to the 25C. Therefore, to better understand the impact of both 25C and 80C MXene nanoparticles on the epoxy's properties, a comprehensive investigation assessment of the tribological. and mechanical properties of the MXene-epoxy nanocomposites will provide more valuable conclusions.

3.3. Micro-CT of MXene-based nanocomposites

The void analysis conducted via micro-CT scanning provided insights into the influence of MXene concentration on the void characteristics in the polymer composites. As significant defects in nanocomposites, voids often appear within the polymeric matrix, forming during the mixing process when the system's viscosity impedes air release [45]. These voids can compromise the performance of the composites, and the nanofiller-polymer interaction can exacerbate or mitigate this by respectively increasing or decreasing voids.

As presented in 3-D transparent images of pure epoxy in Fig. 5, the pure epoxy sample revealed nonporous structures with notable-sized voids. Large void formation in epoxy networks may be attributed to impeded air release, a consequence of the system's viscosity during the mixing process. These substantial voids can jeopardize the composite's integrity, potentially initiating stress concentrations, diminishing the effective load-bearing capacity, and possibly accelerating the process of material failure. As illustrated in Fig. 6, the representative 3-D transparent images of 1.0% 80C-E clearly shows significantly fewer voids compared to the neat epoxy. Moreover, as shown in Fig. 6, the typical layers of samples with 80C MXene were used as examples, providing a clear representation of the microstructure of the composites at various MXene concentrations. Such images significantly contribute to our understanding of the influence of MXene on the microstructure of epoxy composites.

The collected images from Micro-CT visually attest to the efficiency of MXene in reducing voids within the epoxy composite, validating the quantitative results from Table 1. Firstly, the void fraction was noted to reduce remarkably upon the addition of both types of MXene flakes. The neat epoxy exhibited a void percentage of 1.89%, whereas the addition of 0.1% 80C-E MXene culminated in a void percentage of just 0.67%. This trend of decreasing void fraction continued down to 0.02% with the addition of 1.0% 80C-E MXene, confirming the ability of MXene to reduce voids in the epoxy matrix effectively. The reductions in the void fraction can be attributed to the nanoscale size and shape of MXene particles that allow them to fill gaps within the polymer matrix, thereby minimizing void formation. Notably, the 25C MXene samples, much like the 80C samples, demonstrated a remarkable decrease in void percentage upon their addition to neat epoxy. Specifically, the void percentage in neat epoxy was reduced to just 0.80% with the addition of 0.1% 25C-E MXene. This trend of decreasing void fraction continued down to 0.19% with the addition of 1.0% 25C-E MXene. However, the observed reduction in void fraction reached a turning point with both 2.0% 80C and 25C MXene addition,

where the void percentage rebounded to 0.72% and 0.91%, respectively. This trend suggested a delicate balance in MXene nanofiller addition: while low concentrations of MXene enhance the composite's structure by reducing voids, excessive concentrations may induce agglomeration of the nanofiller and entrapped air. The agglomeration of MXene nanofillers increases system viscosity, leading to larger voids and a greater void fraction, a phenomenon that aligns with the previous observations.

The effect of MXene concentration also affecting the size of the voids; for example, the largest size void in the neat epoxy was significantly reduced from 0.608 mm^2 to 0.135 mm^2 with the addition of 0.1% 80C-E MXene, reaching a minimum at 1.0% 80C-E MXene with a size of 0.023 mm^2. However, the largest size void increased to 0.203 mm^2 when 2.0% 80C-E MXene was added, confirming the previous interpretation about the effect of excessive MXene concentration on voids in composites.

These findings indicate that both 25C and 80C MXene, with their exceptional reinforcing capabilities, have the potential to significantly enhance polymer composites' performance by mitigating void formation. Comparing both MXene types, the 80C MXene samples outperformed the 25C samples in reducing the void percentage at equivalent concentrations. This observation can be attributed to the smaller particle size and higher purity of the 80C MXene variant, further emphasizing the role of MXene fabrication method on its efficacy as a nanofiller. However, this positive impact relies on maintaining an optimal MXene concentration to prevent nanofiller agglomeration and reinforce composite microstructure.

(a) (b)

Figure 5. Transparent 3-D images obtained by Micro-CT for (a) neat epoxy and (b) sample with 1% of 80C MXene.

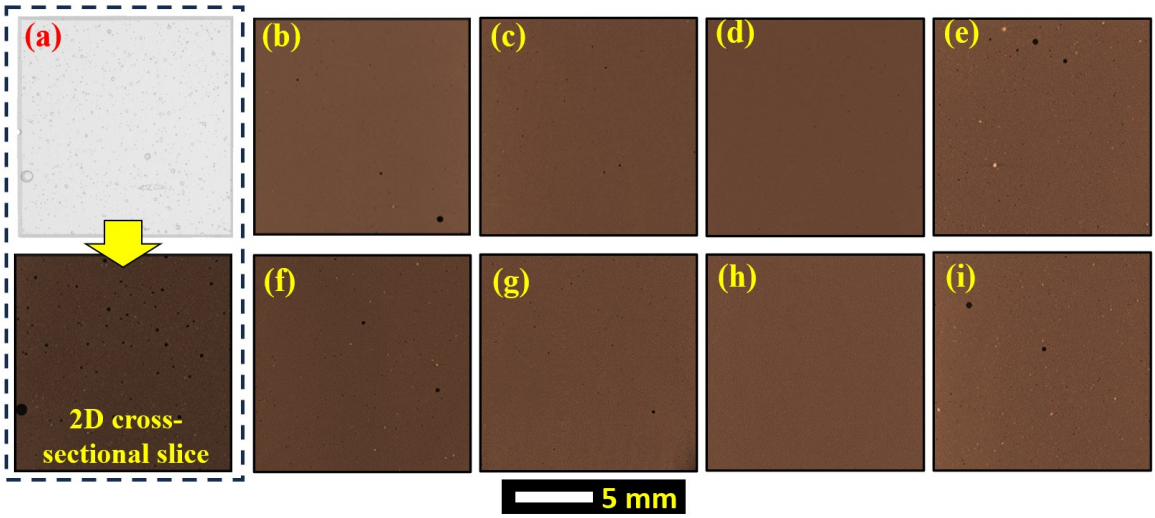

Figure 6. Typical cross-sectional images obtained by Micro-CT, (a) neat epoxy, (b) to (e) samples containing 0.1, 0.5, 1.0 and 2.0 wt.% of 25C MXene, (f) to (i) samples containing 0.1, 0.5, 1.0 and 2.0 wt.% of 80C MXene.

316
317 Table 1. Void parameters of MXene-epoxy composites

Sample group	Void percentage	Largest size of voids (mm^2)	Average size of voids (mm^2)	Standard deviation (mm^2)
Neat epoxy	1.89%	0.608	0.033	0.056
0.1% 25C-E	0.80%	0.203	0.012	0.024
0.5% 25C-E	0.30%	0.065	0.013	0.008
1.0% 25C-E	0.19%	0.023	0.013	0.005
2.0% 25C-E	0.91%	0.180	0.015	0.018
0.1% 80C-E	0.67%	0.135	0.014	0.014
0.5% 80C-E	0.08%	0.045	0.012	0.012
1.0% 80C-E	0.02%	0.023	0.013	0.008
2.0% 80C-E	0.72%	0.203	0.014	0.021

318
319 ***3.4. Mechanical properties of MXene-based nanocomposites***

320 The tensile properties of epoxy composites containing 25C and 80C MXene nanoparticles were
321 investigated, with the results revealing the influence of the MXene particles with unique 2D morphology on the
322 material's performance. As presented in Fig. 7(a), the results demonstrate that the addition of MXene
323 nanoparticles enhances the tensile strength compared to pure epoxy. Clearly, the tensile strength improvement
324 is concentration-dependent and varies between the two types of MXene nanoparticles. This enhancement may
325 be attributed to the strong interfacial interactions between the MXene nanoparticles and the epoxy matrix, which
326 can result in a more efficient stress transfer between the materials.

327 For the epoxy containing 25C MXene nanoparticles, the tensile strength increased by 26% from the pure
328 epoxy at 0.1% concentration, and the strength continued to increase, reaching a peak improvement of 72% at

2.0% concentration. In comparison, the samples containing 80C MXene nanoparticles showed an even more significant enhancement in tensile strength. In the sample with 0.1% of 80C MXene, the tensile strength increased by 28% from the pure epoxy; and the improvement continued to rise with increasing concentration, reaching its highest value of 86% at 2.0% concentration. Apparently, it can be concluded that the tensile strength of the nanocomposites increases with the concentration of both types MXene nanoparticles. This trend suggests that a higher nanoparticle concentration leads to a stronger reinforcing effect; the reinforcement provided by the nanoparticles compensates for the impact of the increased defects within the nanocomposite, as evident from the Micro-CT results (Fig. 6). On the other hand, the tensile strength improvement is more significant for the samples containing 80C MXene nanoparticles, particularly at higher concentrations, which may be due to differences in the properties of the two types of MXene nanoparticles. The tensile strength results for MXene-epoxy composites reveal a clear influence of MXene nanoparticle type and concentration on mechanical performance. The 25C MXene, when added to epoxy, consistently improves tensile strength, with the highest gains observed at a 2.0% concentration. The 80C MXene, characterized by smaller particle size and higher purity (as confirmed in XRD and SEM results), demonstrates a more significant enhancement in tensile strength across all concentrations. This variant's superior performance is likely due to its greater surface area, which facilitates better stress distribution and interfacial bonding within the composite. The 80C MXene's improved dispersion and reduced impurity-related defects, making it offer stronger reinforcement on mechanical strength of epoxy composite.

Different behaviors were observed in the failure strain; for both types of composites, the failure strain reaches a maximum value at specific concentrations (1.0 wt.%) before decreasing (Fig. 7(b)). For the samples containing 25C MXene nanoparticles, the failure strain increased from 2.9% (pure epoxy) to 4.3% with the addition of 0.1wt.% 25C MXene, representing a 48% improvement. The failure strain continued to rise with increasing concentration, reaching its highest value of 6.9% at 1.0 wt.% concentration. However, at 2.0 wt.% concentration, the failure strain slightly decreased to 6.4%, but still shows a 117% improvement compared to pure epoxy. The decrease in failure strain observed in the high-concentration group signifies that the amplified presence of voids establishes a concentrated load location, rendering it more susceptible to fracture under tensile load. In comparison, the sample groups containing 80C MXene nanoparticles showed a more significant enhancement in failure strain. At 0.1 wt.% concentration, the failure strain increased to 4.2% from the pure

epoxy value. The improvement continued to rise with increasing concentration, reaching its highest value of 7.9% at 1.0 wt.% concentration; and similar to the 25C group, the failure strain decreased slightly to 7.3% at 2.0 wt.% concentration.

It is worth noting that the epoxy composites with a 2.0% filler concentration, processed at both 25°C and 80°C, exhibit the highest tensile strengths. However, for achieving the maximum failure strains, the optimal filler content in the epoxy composites processed is identified as 1.0%. Apparently, the tensile strength of a composite material is primarily determined by the load transfer efficiency from the matrix to the reinforcing filler, which in this case are the MXene particles. For the 2.0%-25C-Epoxy and 2.0%-80C-Epoxy composites, the high concentration of MXene likely creates a dense network of nanoparticles, which can efficiently carry the applied load, resulting in higher tensile strength. On the other hand, the failure strain is a measure of the material's ductility, or its ability to deform under tensile stress [46]. At 1.0% filler addition, both the 25C and 80C MXene-epoxy composites exhibit the highest failure strains. This optimal filler concentration strikes a balance between reinforcement and the composite's ability to deform. At this level, there is likely enough MXene to enhance the mechanical properties without causing excessive stiffness or brittleness. As the concentration of MXene increases beyond the optimal level, it's possible that the nanoparticles begin to agglomerate, leading to stress concentrations and a decrease in the composite's ability to deform. This is reason that at 2.0% concentration, while the tensile strength is increased due to higher load transfer capability, the failure strain may not be at its peak because the material becomes more brittle with higher filler content.

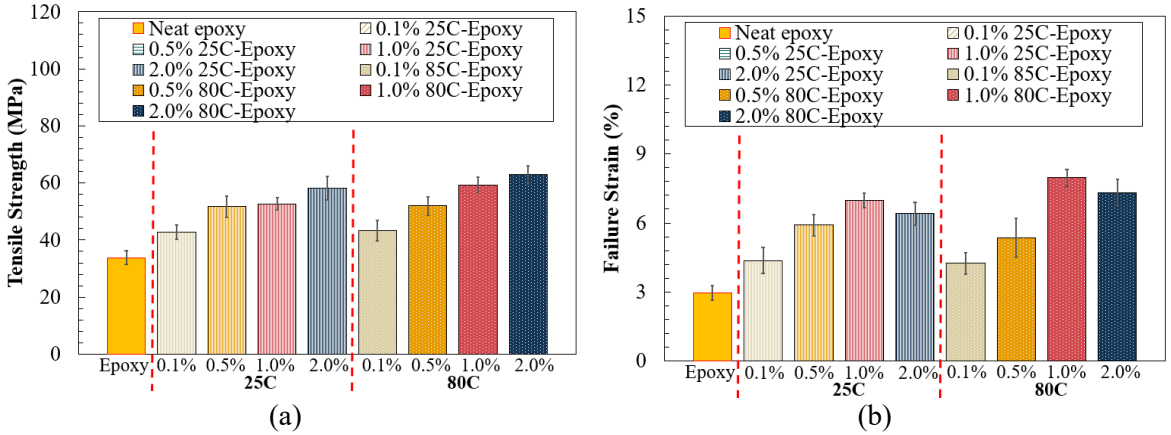

Figure 7. Tensile properties of MXene-epoxy composites, (a) tensile strength, and (b) failure strain.

As illustrated in Fig. 8, the Scanning Electron Microscopy (SEM) images of fracture surfaces after tensile test highlighted the influence of MXene nanoparticles on the mechanical behavior of nanocomposites. The

micrographs reveal that the neat epoxy exhibits large fracture features, indicating low toughness and impact resistance. For the MXene-epoxy nanocomposites, a roughened surface with compact crack patterns was observed from, suggesting an increased energy absorption capability and enhanced fracture resistance. From Fig. 8(b), the addition of 0.1% of MXene increase the already showed significant increase in higher surface roughness and compacted cracking cleavages, suggesting the samples had a higher energy absorption and better resistance to fracture. The improvement of the fracture surface continues increased in 0.5 and 1.0% MXene samples, this morphological transformation could be attributed to improved interphase interaction between MXene nanoparticles and the epoxy matrix, which promotes load transfer and energy dissipation ability during tensile deformation, thus boosting mechanical performance. Similar findings were observed in both 25C and 80C MXene sample groups. Additionally, as presented in Fig. 8(e) fracture surface of 2.0% MXene sample slightly changed with slightly increased size of cleavage, which could due to the existence of MXene agglomerates when high amount of MXene are added (Fig. 8(f)), these agglomerates became load concentrated and leading the sample fail when subjected to tensile load, this observation is consistent with the experiment results that strain at failure became lower at 2.0% MXene sample when compare with 1.0% MXene sample groups.

Apparently, the 2D shape of the MXene nanoparticles contributed significant enhancement of tensile properties. More specifically, as the concentration of MXene particles increased, the tensile strength of both 25C and 80C MXene composites improved. However, the failure strain exhibits a non-linear behavior with respect to the concentration, reaching a maximum value at specific concentrations (1.0%) before decreasing. This observation could be due to the agglomeration of MXene particles and voids formation became severe at higher concentrations. The observed tensile properties also correlate with the previously discussed viscosity results. At lower concentrations, the improved dispersion of MXene particles is consistent with the reduced viscosity and enhanced tensile properties. At higher concentrations, the increase in viscosity is indicative of agglomeration and voids, which affects the balance between nanoparticle reinforcement and defects, ultimately determining the composite's performance. Large agglomerates and voids act as stress concentrators within the composite material, providing a location for the initiation and propagation of cracks when subjected to mechanical loading. As a result, the composite becomes more susceptible to failure, and its mechanical properties might not improve as much as expected or might even deteriorate with increasing concentrations of

nanoparticles. Additionally, the comparison between the 25C and 80C MXene composites reveals that the 80C MXene composites exhibit a greater improvement in failure strain at most of the tested concentrations, which majorly due to its higher purity and better dispersion ability. The enhanced dispersion of 80C MXene in epoxy over 25C MXene can be attributed to its smaller particle size (Fig. 3(b) and (c)), which provides a greater surface area to volume ratio, enhancing contact with the resin and promoting more uniform distribution. The refined particle size ensures a broader interface for interaction with the matrix, leading to improved dispersion. Moreover, as confirmed by XRD results, the higher purity of 80C MXene minimizes the presence of impurities and particle agglomeration. These impurities typically disrupt uniform dispersion by creating aggregation points. The absence or reduction of such defects in the 80C MXene facilitates a more homogenous mix within the epoxy matrix, optimizing the composite's overall performance.

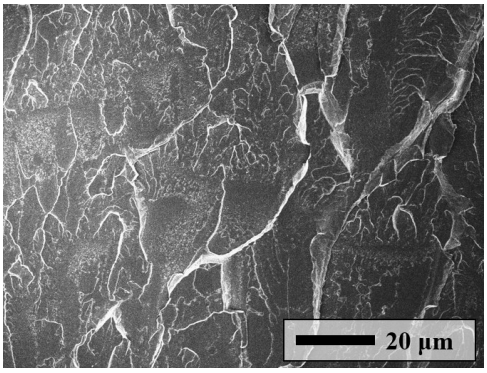

(a) Neat epoxy

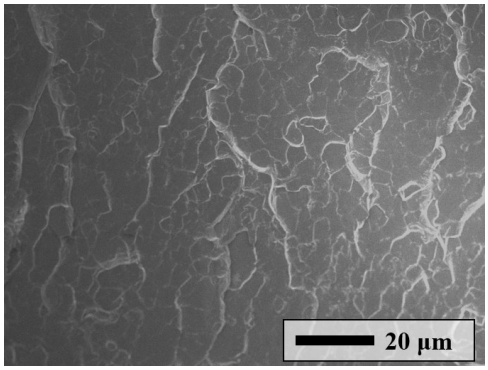

(b) 0.1% 80C MXene-epoxy

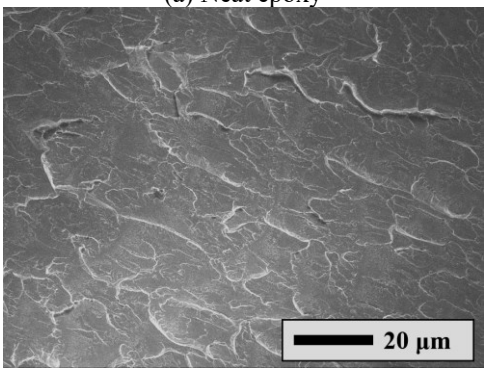

(c) 0.5% 80C MXene-epoxy

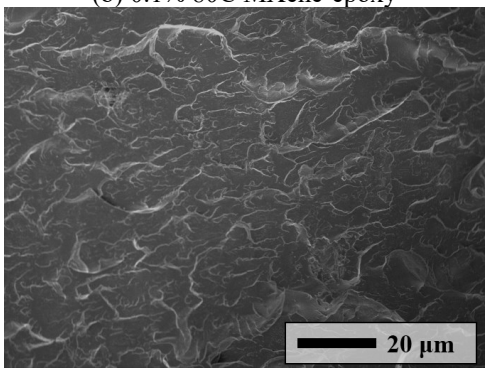

(d) 1.0% 80C MXene-epoxy

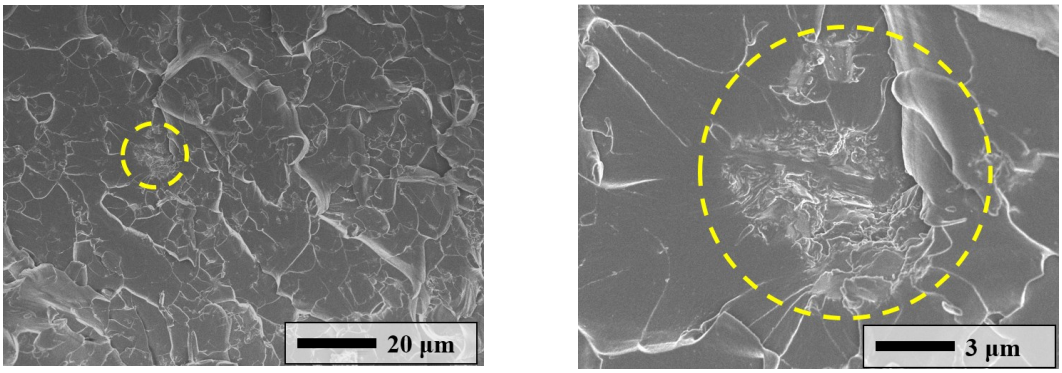

(e) 2.0% 80C MXene-epoxy (f) Aggregated MXene in epoxy

Figure 8. SEM images of fracture surface for (a) neat epoxy, (b) to (e) 80C MXene-epoxy nanocomposite, (f) aggregated MXene in 2.0% of 80C MXene sample.

3.5. Wear resistance of MXene-based nanocomposites

In this section, the abrasion resistance of epoxy composites integrated with 25C and 80C MXene nanoparticles was studied; the mass loss after abrasion testing was used as an indicator of the samples' ability to withstand wear motion. The outcomes (Fig. 9) indicated a noticeable enhancement in abrasion resistance when MXene nanoparticles were introduced into the epoxy matrix, and the abrasion resistance improvement was dependent on the concentration and differs between the two MXene nanoparticle types. For the epoxy containing 25C MXene nanoparticles, the mass loss after abrasion testing decreased 11% when 0.1 wt.% MXene was added. Furthermore, the improvement in abrasion resistance continued with increasing concentrations, reaching 23% reduction in mass loss at 0.5 wt.% and 81.4% at 2.0 wt.% concentration. Similarly, for the epoxy containing 80C MXene nanoparticles, the mass loss after abrasion testing reduced 12% at 0.1 wt.% concentration. Further improvements in abrasion resistance were observed with increasing concentrations, and eventually reached to 83.8% mass-loss reduction at 2.0% concentration.

The enhanced abrasion resistance can be attributed to the reinforcing effect of the MXene nanoparticles; moreover, the unique 2D structure of MXene nanoparticles may provide better load transfer and dissipation of stresses, and contributing to the improved abrasion resistance. Comparing the two types of MXene nanoparticles, the epoxy composites containing 80C MXene exhibited greater improvements in abrasion resistance at all concentration levels, with the highest improvement observed at 2.0. wt.% concentration. The difference in abrasion resistance between the 25C and 80C MXene composites could be due to their particle size and interactions with the epoxy matrix. In conclusion, the addition of MXene nanoparticles, particularly the 80C MXene, significantly improves the abrasion resistance of epoxy composites, indicating the potential of

MXene nanoparticles as effective reinforcements for the development of high-performance epoxy composites with enhanced wear resistance.

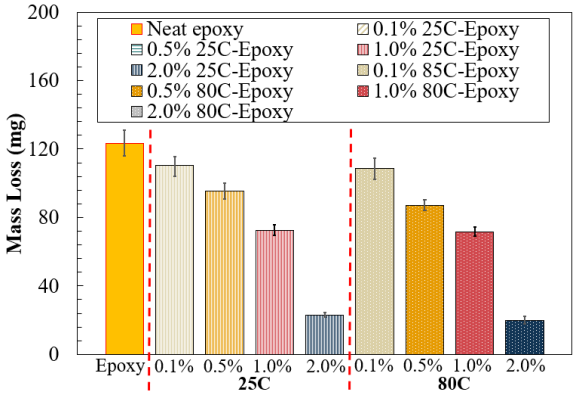

Figure 9. Mass loss of MXene-epoxy nanocomposite after abrasion test.

Fig. 10(a) displays the worn surfaces of both the pure epoxy and the nanocomposites; a notably rougher surface was evident on the pure epoxy sample, characterized by a significant presence of micro-cracks and fractures [47]. This observation suggested that the pure epoxy coating was subjected to plastic deformation and possessed low wear resistance. In the case of pure epoxy, it generates a large number of adhesive debris after friction due to the serious plastic deformation of epoxy, which means the epoxy and abrasive wheels directly slide each other, which leads to high friction coefficient and large wear loss.

In contrast, as depicted in Fig. 10(b), the MXene composites exhibited superior performance based on the surface profiles. A reduction in both the number and size of micro-cracks was observed across all MXene-epoxy systems, which indicates an enhancement in abrasion resistance. Compared with the MXene with different concentrations, it is apparent that the micro-crack reduced with the increased amount of MXene, also the adhesive debris on the abraded surface reduced; and the smoothest surface after abrasion was observed in the 2.0% sample, which showed a good agreement with the results as the 2.0% sample has highest abrasion resistance. Apparently, the inclusion of MXene nanosheets in the coating acts as a load-bearing agent, effectively reducing the strain experienced by the coating, therefore, the friction load can be affectively transferred from the surface to the matrix below through the MXene [48]. Additionally, MXene-epoxy composite and abrasive wheel result in the formation of a uniform and dense lubricating protective film, which can decrease friction and avoid direct contact between the epoxy composite and its counterpart, as well as protect the epoxy composite from severe wear [14,49].

Additionally, the surface roughness of the sample after abrasion test was measured, the surface roughness data after abrasion testing indicates a clear trend: the inclusion of MXene nanoparticles within the epoxy matrix leads to a reduction in surface roughness, which is a proxy for improved abrasion resistance. This trend is consistent across both types of MXene nanoparticles (25C and 80C), with the roughness decreasing as the concentration of MXene increases. The neat epoxy sample had the highest roughness, signifying the least abrasion resistance. With the addition of MXene, the surface roughness reduces significantly. For instance, with just 0.1% of 25C MXene, the roughness is significantly reduced, and this improvement is more pronounced at 2.0% concentration, reducing the roughness to 0.39 μm. This indicates that even a small amount of MXene can impact the wear characteristics of the composite positively, and higher concentrations continue to fortify the composite's surface. Similarly, the 80C MXene variants exhibit an analogous pattern; additionally, the 80C MXene appears to be slightly more effective than the 25C type in improving the wear resistance of the epoxy composites, as evidenced by a lower surface roughness at equivalent concentrations.

The decrease in surface roughness with MXene addition can be related to the material's ability to act as a solid lubricant and to distribute the stress during the abrasion test more evenly. Additionally, the smaller particle size and higher purity of the 80C MXene may contribute to a more homogenous distribution within the epoxy matrix, further reducing the surface roughness. Overall, these findings corroborate the abrasion test results previously discussed, where the MXene-epoxy composites exhibited less mass loss compared to the Neat Epoxy. The surface roughness data adds an additional layer of understanding to the composites' wear characteristics, showing a strong correlation between MXene concentration and the improvement of abrasion resistance.

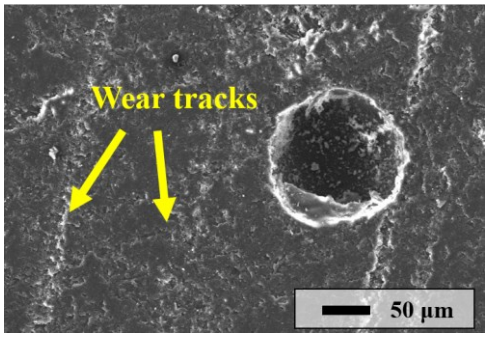

(a) Neat epoxy

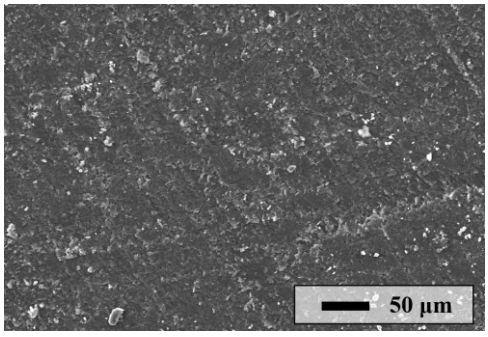

(b) 0.1% 80C MXene

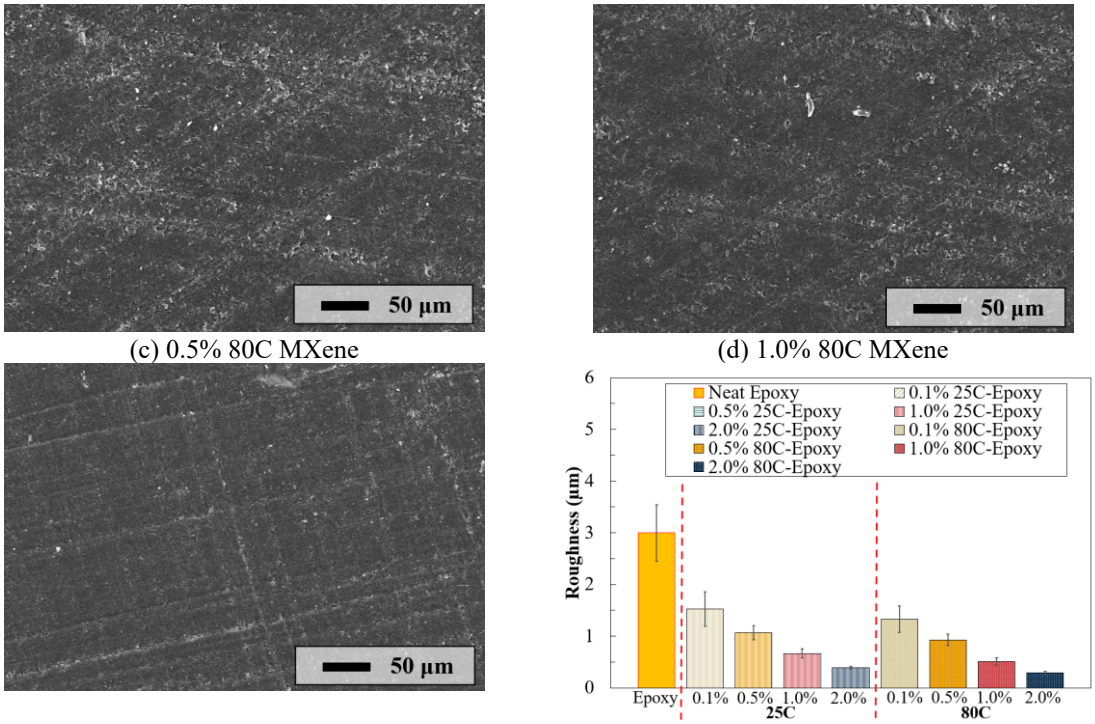

(c) 0.5% 80C MXene (d) 1.0% 80C MXene

(e) 2.0% 80C MXene (f) Surface roughness after abrasion test

Figure 10. SEM images of coatings after abrasion test, (a) pure epoxy, and (b) to (e) 80C MXene epoxy sample. (f) surface roughness of the surface after abrasion test.

3.6. Anti-aging properties of MXene-based nanocomposites

Epoxy is a type of polymer that is commonly used in adhesives, coatings, and composite materials, and it is known for its excellent mechanical and chemical resistance; however, epoxy is also susceptible to degradation by UV light and other natural environment conditions. The aging process can induce the generation of free radicals, which are chemical species distinguished by unpaired electrons; therefore, the presence of these radicals can instigate chain reactions that lead to significant material degradation [50]. As the reactions progress, the structural integrity of the polymer network can be further compromised. Therefore, to evaluate the durability of MXene-based composite under natural weathering (including UV light, heat, and moisture), the specimens were subject to QUV Accelerated Weathering Tester, and the ageing process was characterized by Electron Spin Resonance (ESR) test. In analyzing the gathered ESR data, the free radical concentration in a sample can be estimated by using the formula:

$$I \propto Y'_m(\Delta H_{pp})^2 \quad (1)$$

where $2Y'_m$ represents the peak-to-peak amplitude, ΔH_{pp} defines the distance between the peaks in the sample spectrum, and I is the signal strength [50]. As represented in Fig. 11, due to the consistent peak-to-peak

494 width in all the tested samples, there was a direct correlation between the peak-to-peak ($2Y'_m$) and the
495 concentration of free radicals [3]. To streamline the comparison process, the amplitude of the pure epoxy sample
496 is established as a baseline (100%), and the amplitudes of the other samples were calculated relative to this
497 standard.

498 The results presented a clear view of the correlation between the degree of aging in the MXene-epoxy
499 composite materials and the concentration of MXene added. The neat epoxy showed the highest presence of
500 free radicals, a clear indication of the aging process instigated by QUV exposure. This elevated presence of free
501 radicals correlates with accelerated material degradation, primarily due to the oxidation reactions that these
502 radicals facilitate. However, the incorporation of MXene into the epoxy matrix has a notable effect in reducing
503 the formation of free radicals. With a 0.1% concentration of 80C MXene, the formation of free radicals was
504 reduced to 85%. Interestingly, further increment of MXene concentration to 0.5% and 1.0% led to a more
505 substantial reduction of free radicals, down to 34% and 20%, respectively, suggesting that higher concentrations
506 of MXene up to a certain point can effectively suppress the generation of aging-induced free radicals. In contrast,
507 the 2.0% MXene sample only marginally improved upon the 1.0% result, with free radicals reduced to 22%.
508 This suggests that beyond a certain concentration threshold, the efficiency of MXene as a radical inhibitor seems
509 to be degraded; this observation was plausibly caused by the agglomerations and voids in the composite that
510 containing excessive amounts of MXene, which providing more pathways for oxygen molecules to diffuse into
511 the composite. This situation could potentially enhance the oxidation reactions, therefore, lead to the
512 degradation process of the composite.

513 The findings align well with the earlier results from void analysis, suggesting that while MXene effectively
514 mitigates the aging process in the epoxy, a balance needs to be struck in terms of MXene concentration to
515 maximize its beneficial effects and to avoid the risk of introducing new defects. Overall, these results emphasize
516 the potential of MXene as an effective nanofiller in polymer composites, capable of enhancing their resistance
517 to aging.

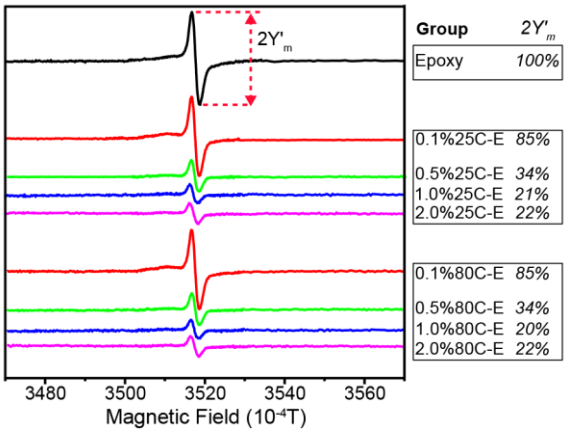

Figure 11. ESR spectra measurement of samples after exposure to accelerated environment

518

519 ***3.7. Material degradation of MXene-based nanocomposite after QUV aging***

520 The Dogbone tensile tests were conducted after QUV accelerated weathering exposure to further validate

521 the anti-aging performance of MXene-epoxy composites, and the results were summarized in Fig. 12. Notably,

522 both the tensile strength and strain for pure epoxy demonstrated substantial reductions, with 32.9% and 34.3%

523 decreases respectively after 500 hours of QUV exposure. This reinforces the conclusion discussed in the ESR

524 results, as epoxy was subject to significant performance degradation upon exposure to harsh environmental

525 conditions, as demonstrated by the free radical formation.

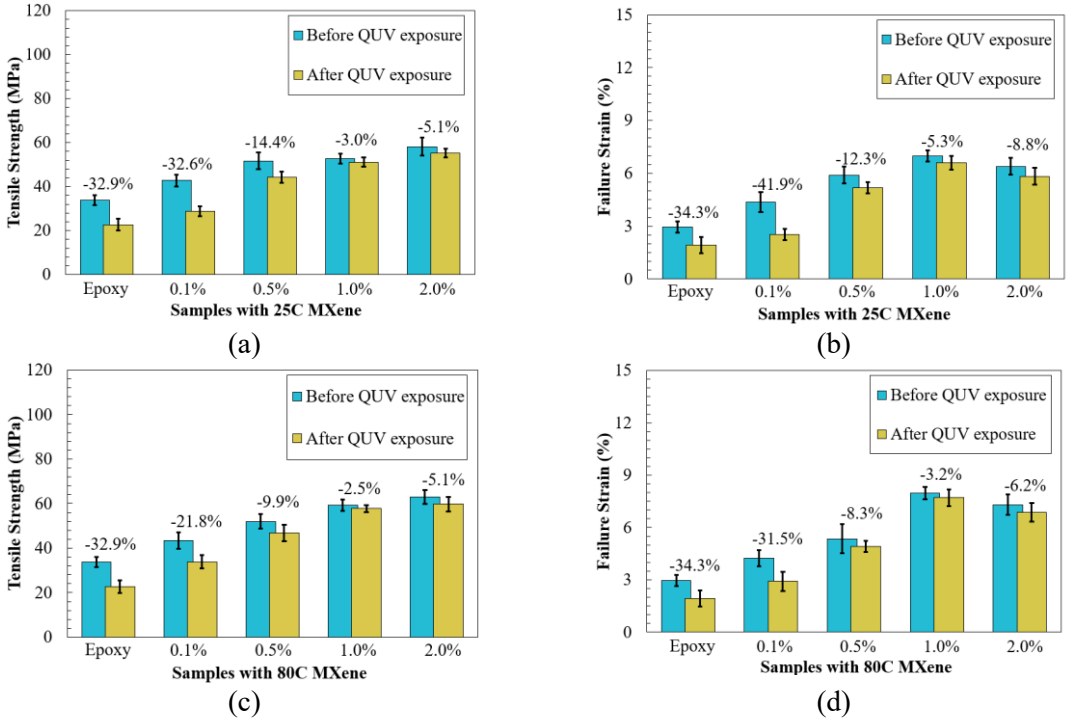

Figure 12. Tensile properties of MXene-epoxy composites after exposure to QUV condition, (a) (c) tensile strength, and (b) (d) failure strain.

The incorporation of 25C MXene and 80C MXene into the epoxy matrix showed obviously different behaviors. With these additives, both tensile strength and strain reductions observed post-QUV exposure were substantially less than those of the pure epoxy. Particularly, with the addition of 1.0% 80C MXene, the reductions in tensile strength and strain were as low as 2.5% and 3.2%, respectively. This observation suggested that the MXene reinforcement significantly mitigates the QUV-induced degradation of the epoxy composites. Furthermore, it is worth noting that 80C MXene exhibits a generally stronger capacity to mitigate the reduction in properties across all tested concentrations when compared to 25C MXene. The observed performance differences between the 25C and 80C MXene variants can be attributed to their respective purities and also the voids in the composite. The 80C MXene, with its higher purity and stronger ability to mitigate the voids, appears to offer enhanced anti-aging properties compared to the 25C variant.

The Scanning Electron Microscopy (SEM) images provided deeper insight into the degradation effects of QUV exposure on both pure epoxy and MXene-epoxy composite samples. The images are particularly useful in illustrating the damage caused by aging and related photodegradation processes at a microscale level. For the pure epoxy sample, the SEM images clearly showed numerous micro-cracks were visible on the fracture surface of the tensile test samples. The presence of such defects on a crucial structural component provides direct evidence of the detrimental impact of QUV-induced aging on the mechanical integrity of the epoxy material. The generation of these cracks can be ascribed to the chemical decomposition of the epoxy matrix under the effects of UV light and other weathering factors [51–53]. As the aging process progresses, chemical reactions likely resulted in material degradation. This aligns with our previous findings from the tensile tests and the Electron Spin Resonance (ESR) tests that showed a substantial increase in free radical concentration and reduction in mechanical performance in the pure epoxy sample upon QUV exposure.

In contrast, the MXene-epoxy samples demonstrated significantly better resistance to photodegradation, as evidenced by the lack of similar micro-cracks on their fracture surfaces post-QUV exposure. . As presented in Fig. 13, which are the MXene-epoxy reinforced by 80C, no additional micro-cracks were observed in the MXene-epoxy sample, regardless of the amount of MXene, and similar findings were also observed in 25C sample groups. This observation aligns with our earlier findings showing that MXene can effectively inhibit the generation of free radicals, hence mitigating the aging process and preserving the structural integrity of the

554 composite material even under harsh environmental conditions. Overall, the SEM images further reinforce the
555 conclusion that MXene can provide substantial enhancement in the UV-aging resistance of epoxy composites.

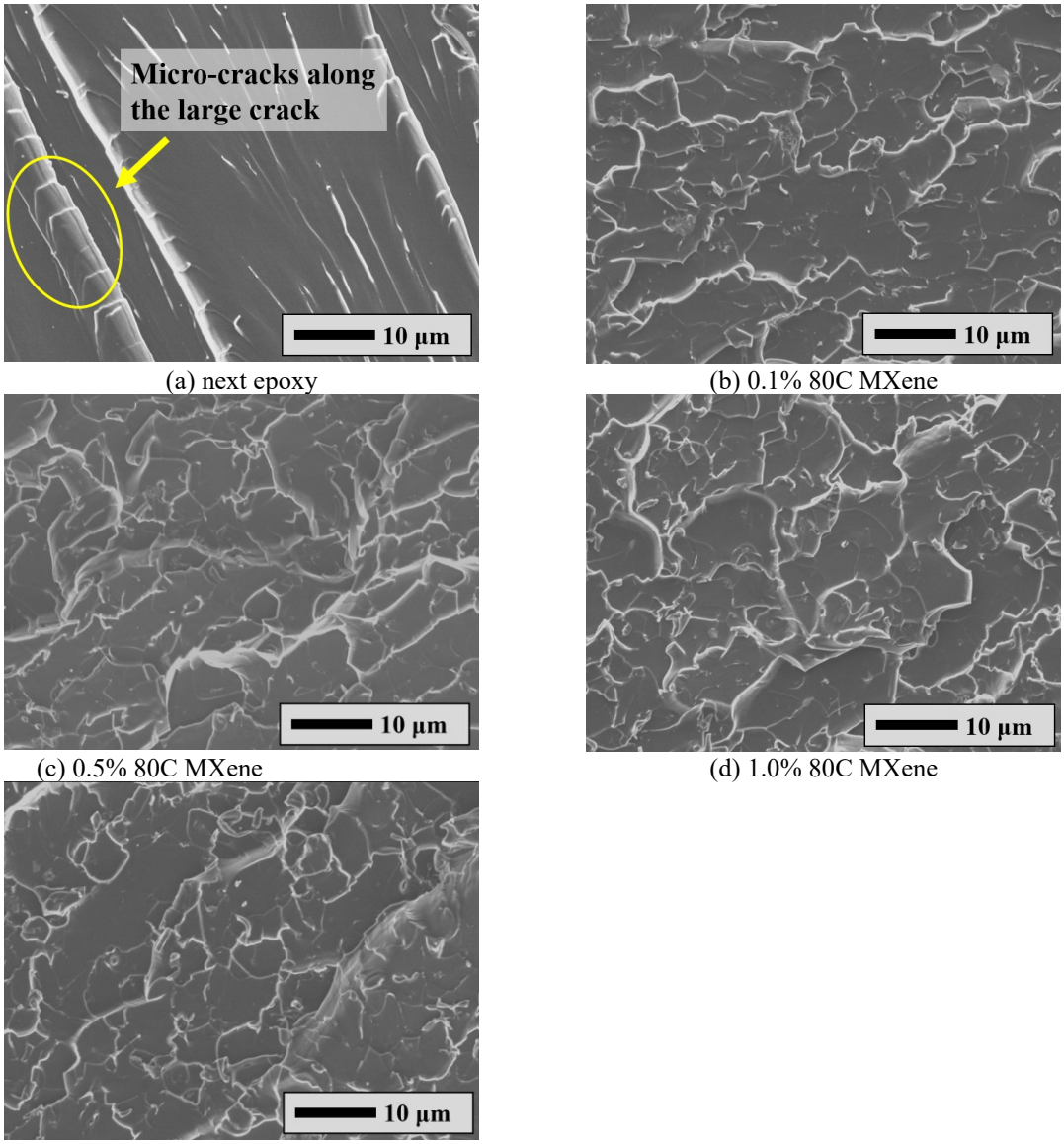

(a) next epoxy (b) 0.1% 80C MXene

(c) 0.5% 80C MXene (d) 1.0% 80C MXene

(e) 2.0% 80C MXene

Figure 13. SEM images of fracture surface after QUV exposure for (a) neat epoxy, (b) to (e) MXene-epoxy nanocomposite.

556

557 The findings of tensile properties after QUV exposure align with the ESR and micro-CT results, where the
558 80C MXene showed superior abilities in reducing free radical formation and minimizing voids within the
559 composite. The trend highlights the correlation between MXene purity, the effective suppression of aging-
560 related degradation, and the overall improved mechanical performance of the composites. Thus, the use of

MXene as a nanofiller in epoxy composites not only enhances their structural integrity but also imparts significantly improved resistance to environmental aging effects.

4. Conclusion

In conclusion, this comprehensive study has revealed the significant promise of MXene nanofillers, produced via two distinct methods (25C and 80C), in enhancing the performance of epoxy-based composites. The research demonstrated that the incorporation of MXene could notably improve the mechanical strength, anti-wear characteristics, and aging resistance of the epoxy matrix, while simultaneously mitigating void formation.

Most notably, the inclusion of 1.0 wt.% MXene effectively eliminated void content in the composite structure. Furthermore, the amplification of tensile strength and anti-wear characteristics reached their peak at 2.0 wt.% MXene, underscoring the necessity of precise MXene concentration management to achieve optimal composite properties. However, it is worth noting that a high concentration of MXene (2.0 wt.%), beyond the optimal levels, could result in an undesired increase in the size and number of voids and potential agglomeration. Our findings also demonstrated the differences between the 25C and 80C MXene variants. The 80C variant, owing to its smaller particle size and higher purity, showed marginally superior reinforcement effects on the epoxy composite. Most significantly, the 1.0 wt.% 80C-MXene sample exhibited remarkable aging resistance, with an 80% reduction in free radical production after QUV exposure, thereby preserving the composite's performance under demanding environmental conditions.

In summary, the findings in this manuscript provide essential insights into the potential of MXene as a nanofiller in epoxy composites, setting a firm foundation for its broader integration into other polymeric systems. These advancements offer new avenues for developing high-performance materials tailored for a diverse range of industrial applications. The results also emphasized the critical role of precise nanofiller concentration management in striking an optimal balance between the desired material enhancements and the potential risk of defects in composite structures.

CRediT authorship contribution statement

Xingyu Wang: Conceptualization, Data curation, Investigation, Formal analysis, Methodology, Validation, Writing - original draft, Writing - review & editing. **Sampada Koirala:** Formal analysis, Methodology, Validation, Writing - original draft. **Luyang Xu:** Formal analysis, Methodology, Validation.

Qiaobin Li: Formal analysis, Methodology, Validation. **Danling Wang:** Supervision, Conceptualization, Investigation, Methodology, Validation, Visualization, Writing - review & editing. **Xiaoning Qi**: Formal analysis, Methodology, Validation. **Zhongyu Yang:** Formal analysis, Methodology, Validation**. Ying Huang:** Supervision, Investigation, Writing - review & editing.**, Zhibin Lin:** Supervision, Conceptualization, Investigation, Methodology, Validation, Visualization, Writing - review & editing.

Declaration of competing interest

The authors declare that they have no known competing financial interests or personal relationships that could have appeared to influence the work reported in this paper.

Acknowledgments

This work was partially supported by the U.S. Department of Transportation PHMSA (Grant No. 693JK3250009CAAP, FAR0034731RA, FAR0036312CAAP), the National Science Foundation (CMMI-1750316). The results, discussion, and opinions reflected in this paper are those of the authors only and do not necessarily represent those of the sponsors.

Reference

[1] Gong K, Zhou K, Qian X, Shi C, Yu B. MXene as emerging nanofillers for high-performance polymer composites: A review. Compos Part B Eng 2021;217:108867.
[2] Li X, Wang C, Cao Y, Wang G. Functional MXene materials: progress of their applications. Chem Asian J 2018;13:2742–57.
[3] Giménez R, Serrano B, San-Miguel V, Cabanelas JC. Recent advances in MXene/epoxy composites: trends and prospects. Polymers 2022;14:1170.
[4] Li X, Yin X, Liang S, Li M, Cheng L, Zhang L. 2D carbide MXene Ti2CTX as a novel high-performance electromagnetic interference shielding material. Carbon 2019;146:210–7.
[5] Wang B, Xu Z, Wu H, Huang F, Liu F, Li S, et al. Architecture-inspired N-doped carbon nanotube bridging well-arranged MXene nanosheets toward efficient electromagnetic wave absorption. Compos Part B Eng 2023;257:110669.
[6] Aakyiir M, Yu H, Araby S, Ruoyu W, Michelmore A, Meng Q, et al. Electrically and thermally conductive elastomer by using MXene nanosheets with interface modification. Chem Eng J 2020;397:125439.
[7] Maity N, Dawn A. Conducting polymer grafting: Recent and key developments. Polymers 2020;12:709.
[8] Nair AB, Shamsudeen SP, Joys M, Varghese N. Future Perspectives of Polymer Supercapacitors for Advanced Energy Storage Applications. Polym. Nanocomposites Supercapacitors, CRC Press; 2022, p. 237–57.
[9] Wang X, Lin Z. Robust, hydrophobic anti-corrosion coating prepared by PDMS modified epoxy composite with graphite nanoplatelets/nano-silica hybrid nanofillers. Surf Coat Technol 2021;421:127440.
[10] Zhang Y, Liu X, Zeng L, Zhang J, Zuo J, Zou J, et al. Polymer fiber scaffolds for bone and cartilage tissue engineering. Adv Funct Mater 2019;29:1903279.
[11] Makowiec ME, Gionta GL, Bhargava S, Ozisik R, Blanchet TA. Wear resistance effects of alumina and carbon nanoscale fillers in PFA, FEP, and HDPE polymers. Wear 2022;502:204376.
[12] Zhou X, Guo Y, Zhao F, Shi W, Yu G. Topology-controlled hydration of polymer network in hydrogels for solar-driven wastewater treatment. Adv Mater 2020;32:2007012.

[13] Qin L, Huang X, Sun Z, Ma Z, Mawignon FJ, Lv B, et al. Synergistic effect of sharkskin-inspired morphologies and surface chemistry on regulating stick-slip friction. Tribol Int 2023;187:108765.
[14] Chen Z, Zhang M, Guo Z, Chen H, Yan H, Ren F, et al. Synergistic effect of novel hyperbranched polysiloxane and Ti3C2Tx MXene/MoS2 hybrid filler towards desirable mechanical and tribological performance of bismaleimide composites. Compos Part B Eng 2023;248:110374.
[15] Wu J, Chen Y, Zhang L, Sheng X. Electrostatic self-assembled MXene@ PDDA-Fe3O4 nanocomposite: A novel, efficient, and stable low-temperature phosphating accelerator. J Ind Eng Chem 2023.
[16] He S, Sun X, Zhang H, Yuan C, Wei Y, Li J. Preparation strategies and applications of MXene-polymer composites: a review. Macromol Rapid Commun 2021;42:2100324.
[17] Liu L, Ying G, Wen D, Zhang K, Hu C, Zheng Y, et al. Aqueous solution-processed MXene (Ti3C2Tx) for non-hydrophilic epoxy resin-based composites with enhanced mechanical and physical properties. Mater Des 2021;197:109276.
[18] Wen G, Wen X, Cao H, Bai P, Meng Y, Ma L, et al. Fabrication of Ti3C2 MXene and tetradecylphosphonic acid@ MXene and their excellent friction-reduction and anti-wear performance as lubricant additives. Tribol Int 2023;186:108590.
[19] Zhou F, Ma Y, Chen Y, Zhang L, Sheng X. Triple-function smart anticorrosion composite coating based on graphene and ZIF-8 with excellent pH-responsive self-healing and in vitro antimicrobial properties. Prog Org Coat 2024;186:108007.
[20] Krishnan U, Kaur M, Singh K, Kumar M, Kumar A. A synoptic review of MoS2: Synthesis to applications. Superlattices Microstruct 2019;128:274–97.
[21] Yuan S, Linas S, Journet C, Steyer P, Garnier V, Bonnefont G, et al. Pure & crystallized 2D Boron Nitride sheets synthesized via a novel process coupling both PDCs and SPS methods. Sci Rep 2016;6:1–9.
[22] Shekhirev M, Shuck CE, Sarycheva A, Gogotsi Y. Characterization of MXenes at every step, from their precursors to single flakes and assembled films. Prog Mater Sci 2021;120:100757.
[23] Verger L, Xu C, Natu V, Cheng H-M, Ren W, Barsoum MW. Overview of the synthesis of MXenes and other ultrathin 2D transition metal carbides and nitrides. Curr Opin Solid State Mater Sci 2019;23:149–63.
[24] Meshkian R, Näslund L-Å, Halim J, Lu J, Barsoum MW, Rosen J. Synthesis of two-dimensional molybdenum carbide, Mo2C, from the gallium based atomic laminate Mo2Ga2C. Scr Mater 2015;108:147–50.
[25] Chen X, Zhao Y, Li L, Wang Y, Wang J, Xiong J, et al. MXene/polymer nanocomposites: preparation, properties, and applications. Polym Rev 2021;61:80–115.
[26] Yan H, Cai M, Li W, Fan X, Zhu M. Amino-functionalized Ti3C2Tx with anti-corrosive/wear function for waterborne epoxy coating. J Mater Sci Technol 2020;54:144–59.
[27] Zeng Y, Xiong C, Li W, Rao S, Du G, Fan Z, et al. Significantly improved dielectric and mechanical performance of Ti3C2Tx MXene/silicone rubber nanocomposites. J Alloys Compd 2022;905:164172.
[28] Yan H, Cai M, Wang J, Zhang L, Li H, Li W, et al. Insight into anticorrosion/antiwear behavior of inorganic-organic multilayer protection system composed of nitriding layer and epoxy coating with Ti3C2Tx MXene. Appl Surf Sci 2021;536:147974.
[29] Yan H, Zhang L, Li H, Fan X, Zhu M. Towards high-performance additive of Ti3C2/graphene hybrid with a novel wrapping structure in epoxy coating. Carbon 2020;157:217–33.
[30] Cai M, Fan X, Yan H, Li Y, Song S, Li W, et al. In situ assemble Ti3C2Tx MXene@ MgAl-LDH heterostructure towards anticorrosion and antiwear application. Chem Eng J 2021;419:130050.
[31] Chen Y, Wu Y, Zhao W. Constructing Ti3C2Tx/Carbon fiber hybrids for enhancing the interfacial strength and erosion wear resistance of EP-based composite coating. Carbon 2023;202:196–206.
[32] Li S, Huang H, Chen F, He X, Ma Y, Zhang L, et al. Reinforced anticorrosion performance of waterborne epoxy coating with eco-friendly L-cysteine modified Ti3C2Tx MXene nanosheets. Prog Org Coat 2021;161:106478.
[33] Wu J, Chen Y, Zhang L, Sheng X. Construction of a high-performance anti-corrosion and anti-wear coating based on the MXene@ PTA-Zn (II): Electrochemical/tribological investigations. Prog Org Coat 2023;182:107706.
[34] He X, Wu J, Huang X, Chen Y, Zhang L, Sheng X. Three-in-one polymer nanocomposite coating via constructing tannic acid functionalized MXene/BP hybrids with superior corrosion resistance, friction resistance, and flame-retardancy. Chem Eng Sci 2024;283:119429.
[35] Chen Z, Zhang M, Ren P, Lan Z, Guo Z, Yan H, et al. Enhanced mechanical and tribological properties of epoxy composites reinforced by novel hyperbranched polysiloxane functionalized graphene/MXene hybrid. Chem Eng J 2023;466:143086.

685 [36] Ama O, Sadiq M, Johnson M, Zhang Q, Wang D. Novel 1D/2D KWO/Ti3C2Tx nanocomposite-based
686 acetone sensor for diabetes prevention and monitoring. Chemosensors 2020;8:102.
687 [37] Alhabeb M, Maleski K, Anasori B, Lelyukh P, Clark L, Sin S, et al. Guidelines for synthesis and processing
688 of two-dimensional titanium carbide (Ti3C2T x MXene). Chem Mater 2017;29:7633–44.
689 [38] Lou D, Chen H, Liu J, Wang D, Wang C, Jasthi BK, et al. Improved Anticorrosion Properties of
690 Polyurethane Nanocomposites by Ti3C2T x MXene/Functionalized Carbon Nanotubes for Corrosion
691 Protection Coatings. ACS Appl Nano Mater 2023.
692 [39] Wang X, Tang F, Cao Q, Qi X, Pearson M, Li M, et al. Comparative Study of Three Carbon Additives:
693 Carbon Nanotubes, Graphene, and Fullerene-C60, for Synthesizing Enhanced Polymer Nanocomposites.
694 Nanomaterials 2020;10:838.
695 [40] Wang X, Tang F, Cao Q, Qi X, Pan H, Lin Z, et al. Nano-modified functional composite coatings for
696 metallic structures: Part II—Mechanical and damage tolerance. Surf Coat Technol 2020:126274.
697 https://doi.org/10.1016/j.surfcoat.2020.126274.
698 [41] Wang X, Pearson M, Pan H, Li M, Zhang Z, Lin Z. Nano-modified functional composite coatings for
699 metallic structures: Part I-Electrochemical and barrier behavior. Surf Coat Technol 2020:126286.
700 https://doi.org/10.1016/j.surfcoat.2020.126286.
701 [42] Bragaglia M, Paleari L, Lamastra FR, Puglia D, Fabbrocino F, Nanni F. Graphene nanoplatelet, multiwall
702 carbon nanotube, and hybrid multiwall carbon nanotube–graphene nanoplatelet epoxy nanocomposites as
703 strain sensing coatings. J Reinf Plast Compos 2021;40:632–43.
704 [43] Rafiee M, Nitzsche F, Laliberte J, Hind S, Robitaille F, Labrosse M. Thermal properties of doubly
705 reinforced fiberglass/epoxy composites with graphene nanoplatelets, graphene oxide and reduced-
706 graphene oxide. Compos Part B Eng 2019;164:1–9.
707 [44] Goyat M, Hooda A, Gupta TK, Kumar K, Halder S, Ghosh P, et al. Role of non-functionalized oxide
708 nanoparticles on mechanical properties and toughening mechanisms of epoxy nanocomposites. Ceram Int
709 2021;47:22316–44.
710 [45] Wang X, Lin Z. Morphologic and synergistic effects of GNP/NS binary-filler-based multifunctional
711 coatings with robust anti-corrosion and hydrophobic properties. Prog Org Coat 2021;157:106286.
712 [46] Koch C, Morris D, Lu K, Inoue A. Ductility of nanostructured materials. Mrs Bull 1999;24:54–8.
713 [47] Wang X, Tang F, Qi X, Lin Z. Mechanical, electrochemical, and durability behavior of graphene nano-
714 platelet loaded epoxy-resin composite coatings. Compos Part B Eng 2019:107103.
715 [48] An D, Wang Z, Qin L, Wu Y, Lu S, Yang H, et al. Preparation of MXene/EP coating for promising
716 anticorrosion and superlow friction properties. Prog Org Coat 2023;183:107779.
717 [49] Chen J, Zhao W. Simple method for preparing nanometer thick Ti3C2TX sheets towards highly efficient
718 lubrication and wear resistance. Tribol Int 2021;153:106598.
719 [50] Xia W, Xue H, Wang J, Wang T, Song L, Guo H, et al. Functionlized graphene serving as free radical
720 scavenger and corrosion protection in gamma-irradiated epoxy composites. Carbon 2016;101:315–23.
721 [51] Nikafshar S, McCracken J, Dunne K, Nejad M. Improving UV-Stability of epoxy coating using
722 encapsulated halloysite nanotubes with organic UV-Stabilizers and lignin. Prog Org Coat
723 2021;151:105843.
724 [52] Bazli M, Jafari A, Ashrafi H, Zhao X-L, Bai Y, Raman RS. Effects of UV radiation, moisture and elevated
725 temperature on mechanical properties of GFRP pultruded profiles. Constr Build Mater 2020;231:117137.
726 [53] Alghamdi MN. Performance for fly ash reinforced HDPE composites over the ageing of material
727 components. Polymers 2022;14:2913.
728

Figure Captions

Table Captions